Thermal electronic properties of aluminum under pressure: The role of *sp* to *3d* electron transfer

Nadine Wetta ⓘ* and Jean-Christophe Pain ⓘ

CEA, DAM, DIF, F-91297 Arpajon, France

As a simple metal, aluminum's valence band is usually described as a free-electron gas with three electrons per atom. The discrepancies between the experimental electronic Grüneisen parameter and heat capacity and their free-electron-gas counterparts are usually attributed to electron-phonon coupling. We recently calculated thermal electronic contributions to aluminum's internal energies with our average-atom code PARADISIO and obtained results that contradict this point of view. Our code also pointed out the overlap of the *sp* valence band by the 3*d* one, resulting in an *sp* to *d* electron transfer. Applying Sommerfeld's temperature expansion method to the electron-electron Coulomb part of the internal energy, we relate the electronic Grüneisen parameter, $T = 0$ K isotherm, and thermal contributions to the internal energy to a parameter α describing the fraction of *d* electrons resulting from *p* to *d* transfer. Finally, we find a unique value of this parameter that provides a consistent explanation for the experimental Grüneisen parameter, for $T = 0$ K energy deduced from experimental shock Hugoniot data, as well as for our average-atom thermal contributions to internal energy.

I. INTRODUCTION

The study of matter under extreme conditions is a subject of great interest with important applications to materials science, geophysics, as well as astrophysics. The need for accurate descriptions of thermophysical properties at extreme conditions is augmented by the growth of interest in inertial-confinement-fusion experiments. Understanding the physics of stellar and planetary interiors requires appropriate theoretical models too.

At first sight, the link between aluminum and these subjects is not obvious. Aluminum's interest relies actually on the fact that it is one of the most studied materials under extreme conditions, in relation to both experimental techniques and theoretical methods that could be developed for the above mentioned studies.

Aluminum was found to be a good choice as a reference material in explosive and light-gas-gun driven shock-wave experiments using the impedance matching technique. Indeed, aluminum is an ideal material from the point of view of theoretical studies, and accurate equations of state (EOS) in the pressure-temperature domain relevant for shock experiments are therefore available, which is the main prerequisite for its use as a reference material. Its interest as a standard for laser-induced shock waves too has been pointed out [1].

In addition, aluminum is also the object of various theoretical investigations covering a wide pressure and temperature range, which makes it also attractive as a reference material for theoretical approaches. Aluminum's theoretical investigations include Thomas-Fermi [2], average-atom [3–7], density-functional, and molecular-dynamics [8–15] theories, as well as semiempirical [16–19] methods. Some of them are favorably examined in the light of shock-wave experiments [20].

In the low density off-Hugoniot domain, quantum-molecular-dynamics results agree with isochoric heating experiments in the "isochoric plasma closed vessel" facility [21]. In the warm-dense-matter regime, the path-integral Monte Carlo method proves its usefulness to benchmark EOS [22] in a domain where experiments are still scarce.

Aluminum belongs to the class of simple metals characterized by nearly free *s* and *p* electrons forming their valence band. Actually, aluminum's $T = 0$ K density of free states is perfectly fitted with the free electron gas (FEG) model [23] for which (we will use atomic units throughout the paper)

$$n(\epsilon) = \frac{3Z^*}{2} \frac{\epsilon^{1/2}}{\epsilon_F^{3/2}}, \tag{1}$$

where Z^* is the number of free electrons, equal to 3 for aluminum, and ϵ_F is the Fermi energy given by

$$\epsilon_F = \frac{1}{2}\left(\frac{3\pi^2 Z^*}{V}\right)^{2/3}, \tag{2}$$

V denoting the atomic volume. In the same reference, the temperature dependence of the calculated chemical potential is also found to be very close to that of the FEG model.

According to the latter model, thermal internal electronic energy and electronic heat capacity read respectively, at temperatures $T \ll T_F = \epsilon_F/k_B$, T_F denoting the Fermi temperature and k_B being the Boltzmann constant,

$$E_{\text{int}}^T = \tfrac{1}{2}\Gamma T^2 \tag{3}$$

and

$$C_V(T) = \Gamma T, \tag{4}$$

where

$$\Gamma = \frac{\pi^2}{3} n(\epsilon_F)k_B^2. \tag{5}$$

*nadine.wetta@cea.fr

Experimental heat capacity as well as electronic Grüneisen parameter are, however, not reproduced with these relations. Indeed, at normal density $\rho_0 = 2.7$ g/cm^3, $\Gamma_{\text{FEG}} = 91$ J/(m^3 K^2), which is somewhat less than the experimental [24] $\Gamma_{\text{exp}} = 135$ J/(m^3 K^2) value cited in Ref. [23]. The FEG value for the electronic Grüneisen constant, defined as

$$\gamma_e = -\frac{d\ln E_{\text{int}}^T}{d\ln \rho} \tag{6}$$

is 2/3, which is considerably lower than the measured values. A recent experiment [25] gives $\gamma_e^{\text{exp}} = 1.4 \pm 0.3$ and confirms previous measurements around 1.6 [26,27].

These differences are usually attributed to strong electron-phonon coupling in aluminum. Accounting for these effects, expression (5) should be corrected by a $(1 + \lambda)$ factor, where λ denotes the electron-phonon coupling parameter. According to Ref. [23], experimental values for λ range between 0.38 and 0.45 for aluminum. Choosing $\lambda \approx 0.42$, the corrected Γ agrees with the experimental one. Concerning the electronic Grüneisen parameter, Wallace calculated the volume derivative of the electron-phonon coupling parameter [27] and obtained the corrected value $\gamma_e = 1.63$, which is in excellent agreement with measurements. A very recent study [28] gives $\lambda = 0.46$ for aluminum at $\rho = \rho_0$ and predicts its strong decay with increasing pressure.

Solid aluminum undergoes a sequence of crystallographic fcc $\rightarrow$ hcp $\rightarrow$ bcc transitions under increasing pressure, recently theoretically investigated in relation to electronic structure [29]. Such a transition sequence is common among transition metals. Its occurrence for simple metal aluminum is explained in Ref. [29] by electron transfer from an sp type band to a $3d$ one as compression rises. This work points out the importance of small deviations from the global simple metal picture on aluminum's behavior under pressure.

Our interest in these two latter topics is related to our recent work on aluminum's EOS. For that purpose, our average-atom code PARADISIO [4], based on Liberman's atom-in-jellium model [30], was used to obtain the electronic contributions to the EOS. A description of PARADISIO code is presented in Appendix A. The code has been improved since the version presented in Ref. [4]. The internal electronic energies are now obtained by summing the different contributions, and the electronic pressure by using the relativistic stress-tensor formula [31]. In the case of aluminum, PARADISIO thermal electronic internal energies exhibit a $E_{\text{int}}^T \propto (\rho/\rho_0)^{-1.56}$ behavior at compression up to 2.7, leading to $\gamma_e \approx 1.56$, which is close to the mean experimental electronic Grüneisen constant $\gamma_e^{\text{exp}} \approx 1.6$ [26,27], whose high value is attributed to electron-phonon coupling. Because PARADISIO does not account for this coupling, we have to find another explanation for the calculated high value.

Our calculations also show that the $Z^* = 3$ valence electrons actually include a small fraction of d-like electrons, even at normal density ρ_0, in agreement with Ref. [29]. By d electrons, we mean a d state that has electron density inside the atomic sphere, even if, in aluminum, $3d$ electron density varies as r^4 within the sphere, which is far from a typical localized d state. This deviation from the FEG could explain our PARADISIO results. We expect those additional d electrons to have an effect on the energies by the means of

electron-electron Coulomb interactions, simultaneously with their impact on the fcc $\rightarrow$ hcp $\rightarrow$ bcc crystallographic transition. Proving it is the main purpose of our work. Beside that, this work also provides an opportunity to benchmark our PARADISIO code at low temperature ($T \lesssim 1$ eV), where its relevance is not obvious. At high temperatures, PARADISIO results agree favorably with other theoretical methods such as molecular dynamics and path-integral Monte Carlo [31]. But we can object that the jellium is a too crude approximation for the ionic environment at lower temperature, and therefore question the adequacy of the INFERNO model under these conditions.

In Sec. II, we will apply Sommerfeld's method to the electronic densities in order to obtain a temperature expansion for the electron-electron Coulomb energy in terms of the valence band's composition. We then introduce a model for aluminum's valence band described as a FEG perturbed by an excess of d electrons associated with a deficit of s and p ones, in order to keep $Z^* = 3$ valence electrons. An analytic expression is then obtained for Coulomb contribution to the energy in terms of the fraction α of d electrons coming from a p-type band. In Sec. III, we relate α to the electronic Grüneisen parameter and to the $T = 0$ K isotherm. Finally, in Sec. IV, we find a value for parameter α which explains our calculated thermal energies as well as the experimental electronic Grüneisen constant γ_e and the $T = 0$ K energy deduced from shock Hugoniot data, and show by this simple way that our PARADISIO results can be explained by sp to d transfer under increasing compression.

II. SOMMERFELD'S LOW TEMPERATURE EXPANSION APPLIED TO COULOMB ENERGY

A. Sommerfeld's expansion method

The so-called Sommerfeld expansion [32–34], introduced by Arnold Sommerfeld to put forward his simple heat capacity model for metals, will be largely used in the present paper. It reads

$$\int_{-\infty}^{\infty} H(\epsilon) f(\epsilon) d\epsilon$$
$$= \int_{-\infty}^{\mu} H(\epsilon) d\epsilon + \sum_{i=1}^{\infty} a_i (k_B T)^{2i} \frac{d^{2i-1} H(\epsilon)}{d\epsilon^{2i-1}}\bigg|_{\mu}, \tag{7}$$

where $H(\epsilon)$ is any function that varies smoothly with energy ϵ. Function $f(\epsilon)$ denotes the Fermi-Dirac distribution

$$f(\epsilon) = \frac{1}{e^{\beta(\epsilon-\mu)} + 1}, \tag{8}$$

where $\beta = 1/k_B T$, μ being the chemical potential. Parameters a_i are related to zeta function by

$$a_i = 2(1 - 2^{1-2i})\zeta(2i).$$

The first two give $a_1 = \pi^2/6$ and $a_2 = 7\pi^4/360$. The well-known Sommerfeld low temperature expansion

$$E = \int_0^{\epsilon_F} \epsilon n(\epsilon) d\epsilon + \frac{\pi^2}{6} n(\epsilon_F)(k_B T)^2 \tag{9}$$

for band structure energy is recovered putting $H(\epsilon) = \epsilon n(\epsilon)$ in Eq. (7).

B. Thermal contributions to electron densities

Within the local approximation of density functional theory, the internal energy reads, neglecting exchange-correlation contributions,

$$E = (E_f + E_b) - \frac{1}{2} \iint_{r,r' \leqslant R} \frac{\rho(r)\rho(r')}{|\vec{r} - \vec{r}'|} \, d^3r \, d^3r', \quad (10)$$

where $(E_f + E_b)$ is the sum over one-electron state energies, whose low temperature expression is given by the Sommerfeld expansion

$$(E_f + E_b)_{T=0} + \frac{\pi^2}{6}(k_B T)^2 n(\epsilon_F) + O(k_B T)^4. \quad (11)$$

The remaining double integral in Eq. (10) represents the electron-electron contributions. We propose to apply Sommerfeld's approach to them.

Let us write the electron density $\rho(r)$ as a sum over electronic states labeled by i,

$$\rho(r) = \sum_i \rho_i(r). \quad (12)$$

We then introduce the partial electron density $\rho_i(r, \epsilon)$ of the state i for an energy ϵ,

$$\rho_i(r) = \int_{-\infty}^{\infty} \rho_i(r, \epsilon) f(\epsilon) \, d\epsilon, \quad (13)$$

the Fermi-Dirac distribution function $f(\epsilon)$ being given in Eq. (8).

Applying Eq. (7) with $H(\epsilon) = \rho_i(r, \epsilon)$ yields

$$\rho_i(r) = \int_{-\infty}^{\mu} \rho_i(r, \epsilon) d\epsilon + \frac{\pi^2}{6}(k_B T)^2 \frac{\partial \rho_i(r, \epsilon)}{\partial \epsilon}\bigg|_{\mu} + O(k_B T)^4. \quad (14)$$

Sommerfeld's expansion for the chemical potential μ reads (see Appendix B)

$$\mu = \epsilon_F - \frac{\pi^2}{6} \frac{n'(\epsilon_F)}{n(\epsilon_F)}(k_B T)^2 + O(k_B T)^4. \quad (15)$$

This relation enables one to express $\rho_i(r)$ in terms of the Fermi energy ϵ_F. We obtain

$$\int_{-\infty}^{\mu} \rho_i(r, \epsilon) d\epsilon$$
$$= \int_{-\infty}^{\epsilon_F} \rho_i(r, \epsilon) d\epsilon + \int_{\epsilon_F}^{\mu} \rho_i(r, \epsilon) d\epsilon$$
$$= \rho_i^{T=0}(r) - \frac{\pi^2}{6}(k_B T)^2 \frac{n'(\epsilon_F)}{n(\epsilon_F)} \rho_i(r, \epsilon_F) + O(k_B T)^4 \quad (16)$$

and

$$\frac{\pi^2}{6}(k_B T)^2 \frac{\partial \rho_i(r, \epsilon)}{\partial \epsilon}\bigg|_{\mu} = \frac{\pi^2}{6}(k_B T)^2 \frac{\partial \rho_i(r, \epsilon)}{\partial \epsilon}\bigg|_{\epsilon_F} + O(k_B T)^4, \quad (17)$$

where we have made the approximation, valid at order $(k_B T)^2$,

$$\int_{\epsilon_F}^{\mu} \rho_i(r, \epsilon) d\epsilon \approx (\mu - \epsilon_F) \rho_i(r, \epsilon_F). \quad (18)$$

Finally, the thermal contribution to the partial electron density $\rho_i(r)$ reads

$$\rho_i^T(r) = \frac{\pi^2}{6}(k_B T)^2 \left(-\frac{n'(\epsilon_F)}{n(\epsilon_F)} \rho_i(r, \epsilon_F) + \frac{\partial \rho_i(r, \epsilon)}{\partial \epsilon}\bigg|_{\epsilon_F} \right)$$
$$+ O(k_B T)^4. \quad (19)$$

In the case of an ideal FEG,

$$\frac{n'(\epsilon_F)}{n(\epsilon_F)} = \frac{1}{2\epsilon_F} \quad (20)$$

and

$$\rho(r, \epsilon) = n(\epsilon) = \frac{3Z^*}{2} \frac{\epsilon^{1/2}}{\epsilon_F^{3/2}}, \quad (21)$$

and consequently one finds that $\rho^T(r) = 0$. As expected for the FEG, electron-electron interactions do not contribute to thermal internal energy. This explains the success of Sommerfeld's low temperature expression for simple metals like aluminum. But Eq. (19) suggests possible thermal contributions to the electron-electron Coulomb interactions from bands of higher orbital quantum number crossing the Fermi level.

C. Approximation by spherical wave functions

To carry on with our development, we describe the electronic wave functions as spherical waves:

$$\varphi_i(r) = \left(\frac{2k^2}{\pi}\right)^{1/2} j_\ell(kr), \quad (22)$$

where j_ℓ is the spherical Bessel function of order ℓ. The electronic states are now labeled by the quantum orbital number ℓ instead of i. We also assume that the asymptotic expression

$$\lim_{x \ll \ell(\ell+1)} j_\ell(x) \approx \frac{x^\ell}{(2\ell + 1)!!} \quad (23)$$

for the Bessel functions can be used.

We refer to the $T = 0$ K quantities by superscript 0 and to the thermal contributions by superscript T. The partial electron density $\rho_\ell^0(r, \epsilon)$ behaves then as $A k^2 (kr)^{2\ell}$, where the normalization coefficient A has to fulfill the condition

$$Z_\ell^0 = \int_{r \leqslant R} \int_0^{\epsilon_F} \rho_\ell^0(r, \epsilon) d\epsilon \, d^3r, \quad (24)$$

Z_ℓ^0 representing the number of electrons in the state ℓ. Finally we write

$$\rho_\ell^0(r, \epsilon) = \frac{Z_\ell^0}{4\pi} \frac{(2\ell + 3)^2}{2\epsilon_F^{(2\ell+3)/2} R^{2\ell+3}} \epsilon^{(2\ell+1)/2} r^{2\ell} \quad (25)$$

and

$$\rho_\ell^0(r) = \frac{Z_\ell^0}{4\pi} \frac{(2\ell + 3)}{R^{2\ell+3}} r^{2\ell}. \quad (26)$$

The thermal contribution $\rho_\ell^T(r)$ to the electron density $\rho_\ell(r)$ is then given by

$$\rho_\ell^T(r) = \frac{\pi^2}{6}(k_B T)^2 \left(-\frac{n'(\epsilon_F)}{n(\epsilon_F)} \rho_\ell(r, \epsilon_F) + \frac{\partial \rho_\ell(r, \epsilon)}{\partial \epsilon}\bigg|_{\epsilon_F} \right)$$
$$+ O(k_B T)^4 \quad (27)$$

with

$$\rho_\ell^0(r, \epsilon_F) = \frac{Z_\ell^0}{4\pi} \frac{(2\ell + 3)^2}{2\epsilon_F} \frac{r^{2\ell}}{R^{2\ell+3}} \quad (28)$$

and

$$\left.\frac{\partial \rho_\ell^0(r, \epsilon)}{\partial \epsilon}\right|_{\epsilon_F} = \frac{(2\ell + 1)}{2} \frac{\rho_\ell^0(r, \epsilon_F)}{\epsilon_F}. \quad (29)$$

D. Case of aluminum

We now introduce a simple model for aluminum's valence band. Let us assume that aluminum's actual valence band can be identified as $Z^* = 3$ electrons forming a uniform FEG in the atomic sphere of radius R. The density of states of this system is then

$$n(\epsilon) = \frac{3Z^*}{2\epsilon_F^{3/2}} \epsilon^{1/2}. \quad (30)$$

A proof of the relevance of this assumption can be found in Fig. 1(a) of Ref. [23], where the VASP (Vienna *Ab initio* Simulation Package) electron DOS of aluminum is found to be well averaged by a FEG DOS $n(\epsilon) \approx \epsilon^{1/2}$ assuming $Z^* = 3$ valence electrons. The band structure contribution to the energy is given, at low temperature, by the familiar expansion

$$\frac{\pi^2}{6} n(\epsilon_F)(k_B T)^2 + O(k_B T)^4 \quad (31)$$

and the chemical potential μ by

$$\mu - \epsilon_F = -\frac{\pi^2}{12} \frac{(k_B T)^2}{\epsilon_F} + O(k_B T)^4. \quad (32)$$

We recall the expression of the FEG's Fermi energy,

$$\epsilon_F = \frac{1}{2}\left(\frac{3\pi^2 Z^*}{V}\right)^{2/3}. \quad (33)$$

Let us denote the electron density as

$$\rho_{\text{FEG}} = \frac{3Z^*}{4\pi R^3} = \frac{Z^*}{V} = \frac{(2\epsilon_F)^{3/2}}{3\pi^2}. \quad (34)$$

Suppose now that, by the effect of compression, the bottom of an $\ell = 2$ d band moves down below the Fermi energy ϵ_F, making possible the transfer of a small part of the Z^* electrons on it, and let us introduce the following perturbation to the ideal FEG:

$$\delta\rho(r) = -\delta\rho_0(r) - \delta\rho_1(r) + \delta\rho_2(r). \quad (35)$$

The perturbed electron density is then

$$\rho(r) = \rho_{\text{FEG}} + \delta\rho(r). \quad (36)$$

Under this perturbation the Coulomb contribution to internal energy reads

$$U_c = -\frac{1}{2} \iint_{r,r' \leqslant R} \frac{\rho(r)\rho(r')}{|\vec{r} - \vec{r}'|} d^3r\, d^3r'$$

$$\approx -\frac{1}{2} \iint_{r,r' \leqslant R} \frac{\rho_{\text{FEG}}^2}{|\vec{r} - \vec{r}'|} d^3r\, d^3r'$$

$$- \frac{1}{2} \iint_{r,r' \leqslant R} \frac{\rho_{\text{FEG}}(\delta\rho(r) + \delta\rho(r'))}{|\vec{r} - \vec{r}'|} d^3r\, d^3r', \quad (37)$$

where the perturbation is assumed to be small enough to allow us to neglect $\delta\rho(r)\delta\rho(r')$ terms. Perturbation $\delta\rho(r)$ decomposes further as a cold contribution (i.e., a $T = 0$ K contribution) and a thermal one,

$$\delta\rho(r) = \delta\rho^0(r) + \delta\rho^T(r), \quad (38)$$

with

$$\delta\rho^0(r) = -\frac{3Z_0^0}{4\pi R^3} - \frac{5Z_1^0}{4\pi R^5}r^2 + \frac{7Z_2^0}{4\pi R^7}r^4. \quad (39)$$

The total number of electrons in the valence band remains equal to Z^*, so that

$$Z_2^0 = Z_0^0 + Z_1^0. \quad (40)$$

Equation (27) reads then

$$\delta\rho^T(r) = \frac{\pi^2}{6} \frac{(k_B T)^2}{\epsilon_F}[-\delta\rho_1(r, \epsilon_F) + 2\delta\rho_2(r, \epsilon_F)], \quad (41)$$

where

$$\delta\rho_2(r, \epsilon_F) = \frac{Z_2^0}{4\pi} \frac{49}{2\epsilon_F R^7} r^4 \quad (42)$$

and

$$\delta\rho_1(r, \epsilon_F) = -\frac{Z_1^0}{4\pi} \frac{25}{2\epsilon_F R^5} r^2. \quad (43)$$

After integration over the angular coordinates, we obtain, for the cold contribution (i.e., the $T = 0$ K contribution) to U_c,

$$U_c^0 = \frac{3Z^*}{5}\epsilon_F - 4\pi \frac{3Z^*}{R^3}\left\{\int_0^R r^2 \int_r^R r'\delta\rho^0(r')dr'dr \right.$$

$$\left. + \int_0^R r^2 \delta\rho^0(r) \int_r^R r'dr'dr\right\}, \quad (44)$$

where the first term of the sum comes from the unperturbed FEG and the second from the perturbation. We will note this latter term δU_c^0. Introducing $\delta\rho^0(r)$ [given by Eq. (39)], we get

$$\delta U_c^0 = -\frac{3Z^*}{R}\left(-\frac{2}{5}Z_0^0 - \frac{8}{21}Z_1^0 + \frac{10}{27}Z_2^0\right), \quad (45)$$

and finally, using the constraint $Z_0^0 + Z_1^0 = Z_2^0$, and introducing the fraction $\alpha = Z_1^0/Z_2^0$ of d electrons coming from p states, we get

$$\delta U_c^0 = \frac{2Z^* Z_2^0}{5R}\left(\frac{2}{9} - \frac{1}{7}\alpha\right). \quad (46)$$

The thermal contribution to U_c,

$$U_c^T = -4\pi \frac{3Z^*}{R^3}\left\{\int_0^R r^2 \int_r^R r'\delta\rho^T(r')dr'dr \right.$$

$$\left. + \int_0^R r^2 \delta\rho^T(r) \int_r^R r'dr'dr\right\} \quad (47)$$

is obtained in the same way. Adding it to the familiar Sommerfeld term, which accounts for the energy spectrum, the thermal contribution to the electronic internal energy reads

$$E_{\text{int}}^T = \frac{\pi^2}{6}(k_B T)^2\left[n(\epsilon_F) - \frac{2Z^* Z_2^0}{\epsilon_F^2 R}\left(\frac{35}{9} - \frac{10}{7}\alpha\right)\right]$$

$$+ O(k_B T)^4. \quad (48)$$
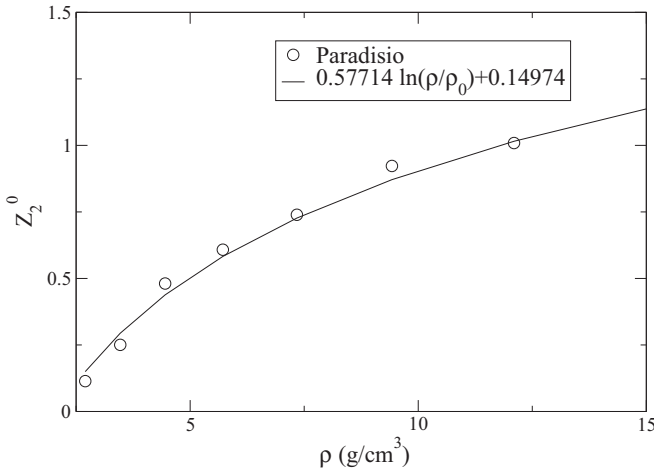
FIG. 1. Fit of the average-atom occupation number of the $3d$ states in aluminum at densities $\rho \geqslant \rho_0$.

FIG. 2. Electronic Grüneisen constant as a function of the fraction α of p electrons that transfer to the d band (straight line). α must be greater than 1.7 to keep γ_e within the experimental uncertainty 1.4 ± 0.3 marked out by the two horizontal dashed lines.

To sum up, we have expressed the contribution to the internal energy of sp-type- to d-type-band electronic transfer in terms of the α fraction of d electrons coming from p-type states and of the resulting Z_2^0 occupancy of the former states. The variation of Z_2^0 with the compression rate can be obtained using our average-atom code. We fitted the results in Fig. 1 by the relation

$$Z_2^0 = 0.57714 \ln(\rho/\rho_0) + 0.14974. \tag{49}$$

We then obtain the parameter α from experimental data, and finally check the consistency of our average-atom thermal electronic contributions to the energy with these data. Before that, we can already give lower and upper bounds for parameter α by remarking that electron-electron Coulomb interactions bring negative U_c^0 and E_{int}^T contributions to the energy. Using Eqs. (46) and (48), we get then

$$\tfrac{14}{9} \leqslant \alpha \leqslant \tfrac{49}{18}, \tag{50}$$

that is

$$1.56 \leqslant \alpha \leqslant 2.72. \tag{51}$$

The fact that parameter α is greater than 1 means that, rather than the expected p to d and s to d transfers, we have actually p to d and p to s ones. Deriving Eqs. (46) and (48), we write $Z_2^0 = Z_1^0 + Z_0^0$ with $Z_1^0 = \alpha Z_2^0$ and $Z_0^0 = (1 - \alpha)Z_2^0$. This is strictly the same as using the most appropriate expressions for p to d and p to s transfers,

$$Z_1^0 = Z_2^0 + Z_0^0 \tag{52}$$

with $Z_2^0 = \widetilde{\alpha} Z_1^0$ and $Z_0^0 = (1 - \widetilde{\alpha})Z_1^0$, where

$$0.4 \lesssim \widetilde{\alpha} = \frac{1}{\alpha} \lesssim 0.6. \tag{53}$$

All the preceding developments rely on the assumption that the perturbation $\delta\rho(r)$ remains small enough to not significantly change the global FEG shape of the DOS. This will be verified *a posteriori* once the parameter α is determined.

III. LINK WITH EXPERIMENTAL DATA

A. Electronic Grüneisen parameter

As mentioned before, electronic Grüneisen parameter is defined as the derivative

$$\gamma_e = -\frac{\partial \ln E_{\text{int}}^T}{\partial \ln \rho}. \tag{54}$$

Applying Eq. (48), we obtain

$$\gamma_e = \frac{2}{3} \times \frac{1 - \frac{2Z_2^0}{\epsilon_F R}\left(1 - \frac{d \ln Z_2^0}{d \ln \rho}\right)\left(\frac{35}{9} - \frac{10}{7}\alpha\right)}{1 - \frac{4Z_2^0}{3\epsilon_F R}\left(\frac{35}{9} - \frac{10}{7}\alpha\right)}, \tag{55}$$

that is, for aluminum at density ρ_0

$$\gamma_e = \frac{2}{3} \times \frac{1 + 0.6676\left(\frac{35}{9} - \frac{10}{7}\alpha\right)}{1 - 0.1559\left(\frac{35}{9} - \frac{10}{7}\alpha\right)}, \tag{56}$$

using Eq. (49) for Z_2^0. According to the most recent experiments from which

$$\gamma_e^{\text{exp}} = 1.4 \pm 0.3, \tag{57}$$

the interval given by Eq. (50) can be further restricted to (see Fig. 2)

$$1.7 \leqslant \alpha \leqslant 2.2. \tag{58}$$

B. Experimental cold curve from shock Hugoniot data

The cold (i.e., the $T = 0$ K isotherm) contributions $E_c(\rho)$, $P_c(\rho)$ to the EOS can be determined from shock Hugoniot data [35–38] assuming a Mie-Grüneisen type EOS

$$P(\rho, E) = P_c(\rho) + \gamma\rho[E(\rho, T) - E_c(\rho)], \tag{59}$$

where γ denotes the Grüneisen coefficient defined as

$$\gamma = \frac{d \ln \Theta}{d \ln \rho}, \tag{60}$$

Θ being the Debye temperature. Replacing P and E by pressure P_H and energy E_H on the Hugoniot curve and using the

preceding definition of γ and the relation $P_c(\rho) = \rho^2 \, dE_c/d\rho$, one gets

$$E_c(\rho) = \Theta(\rho)\left(\frac{E_c(\rho_0)}{\Theta(\rho_0)} + \int_{\rho_0}^{\rho} \frac{P_H(x) - x\gamma(x)E_H(x)}{x^2\Theta(x)} dx\right). \tag{61}$$

To obtain $E_c(\rho)$ from experimental Hugoniot data, one needs a $\gamma(\rho)$ relation and the Debye temperature at density ρ_0. We take the value $\Theta(\rho_0) = 428 \pm 1$ K deduced from low temperature heat capacity [39]. Many $\gamma(\rho)$ relations have been proposed for the purpose of extracting cold curves from Hugoniot data. For aluminum, two expressions emerge. One of them is attributed to Burakovsky and Preston [40] and reads

$$\gamma_{\mathrm{BP}} = \frac{1}{2} + \gamma_1\left(\frac{\rho_0}{\rho}\right)^{1/3} + \gamma_2\left(\frac{\rho_0}{\rho}\right)^n, \tag{62}$$

with $\gamma_1 = 0.6$, $\gamma_2 = 1.4$, and $n = 3.5$. The second relation is the one proposed by Jacobs and Schmid-Fetzer [41],

$$\gamma_{\mathrm{JS}} = \gamma_\infty + (\gamma_0 - \gamma_\infty)\left(\frac{\rho_0}{\rho}\right)^m, \tag{63}$$

with $\gamma_\infty = 0.9$, $\gamma_0 = 2.178$, and $m = 2.15$.

The melting curve obtained assuming a formula for γ is a good test of its adequacy. Nie et $al.$ [42] obtained comparable melting curves with the two expressions, both in excellent agreement with experiments. The two $\gamma(\rho)$ relations can only be discriminated on the basis of the second- and third-order Grüneisen coefficients, which are better recovered with Jacobs's expression. One can also notice that $\gamma_{\mathrm{JS}}(\rho_0) = 2.178$ is closer to the experimental [38] $\gamma_{\mathrm{exp}} = 2.14$ value than $\gamma_{\mathrm{BP}}(\rho_0) = 2.5$. Despite these observations, we used both γ_{BP} and γ_{JS} in Eq. (61). We also tried two other formulations, the first being the so-called Sesame expression [43]

$$\gamma_S(\rho) = \gamma_0\frac{\rho_0}{\rho} + \gamma_\infty\left(1 - \frac{\rho_0}{\rho}\right), \tag{64}$$

with $\gamma_0 = 2.14$ and $\gamma_\infty = 2/3$, and the second the Thompson-Lauson formula [44]

$$\gamma_{\mathrm{TL}}(\rho) = \gamma_0\frac{\rho_0}{\rho} + \gamma_\infty\left(1 - \frac{\rho_0}{\rho}\right)^2, \tag{65}$$

that uses the same γ_0 and γ_∞.

A great number of Hugoniot points are available for aluminum up to density $\rho \approx 6$ g/cm^3. We fitted in Fig. 3 the $P_H(\rho)$ values from Rusbank database [45] and obtained (P_H in GPa and ρ in g/cm^3)

$$P_H(\rho) = 40.934\,\rho^2 - 216.64\,\rho + 291.46. \tag{66}$$

Figure 4 shows the cold pressures $P_c(\rho)$ obtained with the four $\gamma(\rho)$ expressions. The slopes of the cold pressures obtained with γ_S and γ_{TL} tend to decrease at the highest densities $\rho \gtrsim 5$ g/cm^3. As expected according to the work of Nie et $al.$ [42], γ_{BP} and γ_{JS} lead to very close curves, only slightly separating from each other above $\rho \gtrsim 5$ g/cm^3. However, the full red curve corresponding to the best γ according to Nie et $al.$ seems to begin to drop at the highest densities.
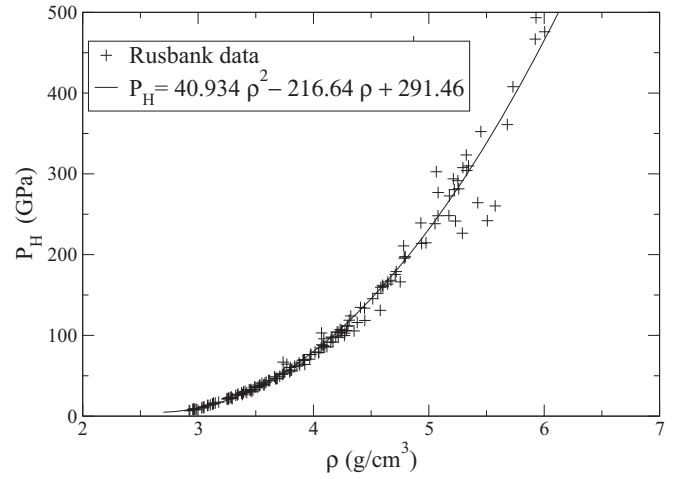
FIG. 3. Fit of Rusbank's data for aluminum.

Figure 5 presents the cold energies $E_c(\rho)$ deduced from Hugoniot data. According to the preceding Fig. 4, we truncated the curves obtained with γ_S and γ_{TL} at 5 g/cm^3.

Equation (44) does not include contributions from bound electrons. We used therefore the energy obtained with the (orbital free) Thomas-Fermi model as a basis to which add our δU_c^0 corrections [Eq. (46)] from Coulomb interactions. We obtained the best agreement with the experimental curve deduced from Hugoniot data using the lowest limit $\alpha = 1.7$ given by Eq. (58). The result is represented by the crosses and is close to the cold curves obtained using γ_{BP} and γ_{JS}, especially at the highest densities. The agreement is poorer at the lowest densities, but rather good with the two curves obtained with the Sesame and the Thompson-Lauson relations. The circles represent the results obtained with $\alpha = 1.95$ (i.e., the value giving $\gamma_e = 1.4$) and lie sensitively lower.

C. Comments

In Ref. [28], Giri et $al.$ calculate the electron-phonon coupling parameter λ under pressure for aluminum. Their normal
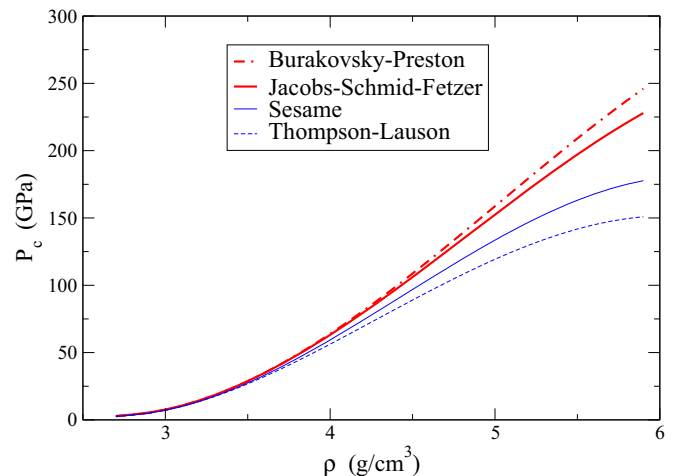
FIG. 4. Pressure at $T = 0$ K deduced from shock Hugoniot data assuming different $\gamma(\rho)$ relations.
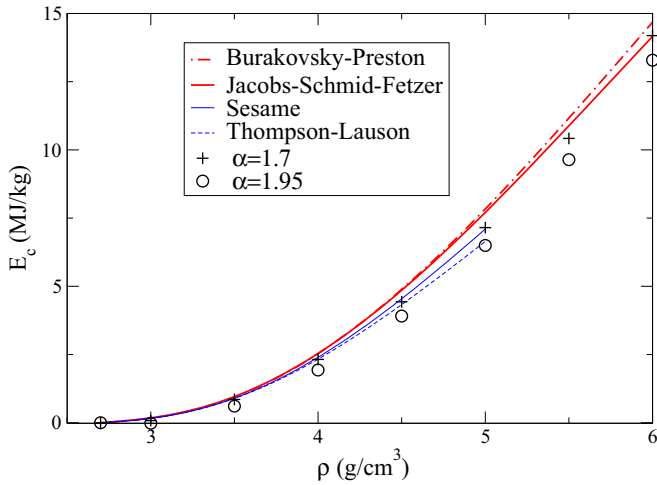
FIG. 5. Internal energy at $T = 0$ K deduced from shock Hugoniot data assuming different $\gamma(\rho)$ relations. Crosses and circles have been obtained using Eq. (46), with respectively $\alpha = 1.7$ and $\alpha = 1.95$.

pressure value $\lambda = 0.46$ confirms a previously published one [23]. At high pressure, the coupling parameter is found to decrease rapidly. From their figures, one can estimate that its value is divided by 2 at $\rho \approx 1.2\rho_0$ ($P \approx 25$ GPa), and falls to $\lambda = 0.12$ at $\rho \approx 1.5\rho_0$ ($P = 82$ GPa).

Our work mainly concerns thermal electronic properties at high compression, where electron-phonon coupling vanishes considerably according to Giri *et al.* In Fig. 5, a unique value is chosen for parameter α within the interval (58) by fitting a high compression quantity, i.e., the $T = 0$ K electronic energy curve up to 6 g/cm^3, deduced from shock experiments. This implies that electron-phonon coupling is neglected at the considered compression rates, which is a reasonable assumption according to Ref. [28], especially above $\rho/\rho_0 \approx 1.5$.

Close to density ρ_0, neglecting electron-phonon coupling is highly questionable. The $\alpha = 1.7$ value that reproduces at best the $T = 0$ K energy curve corresponds to the lowest possible value according to interval (58). The latter interval is based on the assumption that electron-phonon coupling can be omitted. Accounting for these effects is beyond the scope of our simple approach. But we can reasonably think that they will give other intervals for values of α that very probably contain $\alpha = 1.7$ too. Close to ρ_0 (i.e., at $\rho/\rho_0 \lesssim 1.2$), sp to d electron transfer with $\alpha = 1.7$ does not necessary mean that we have to consider that electron-phonon coupling is negligible. Although our approach neglecting electron-phonon coupling is questionable at normal density, we believe that it is globally a reasonable approximation at higher densities, in which we are interested in the present study.

D. Conservation of the global FEG behavior of the DOS

We are now able to verify the validity of our main assumption, i.e., that the $\delta\rho(r)$ perturbation does not induce too much deviation from the FEG $n(\epsilon) \propto \epsilon^{1/2}$ behavior of the valence band. Let us write the perturbed DOS

$$n(\epsilon) = n_{\text{FEG}}(\epsilon) + \delta n(\epsilon) = n_{\text{FEG}}(\epsilon)\left(1 + \frac{\delta n(\epsilon)}{n_{\text{FEG}}(\epsilon)}\right), \quad (67)$$
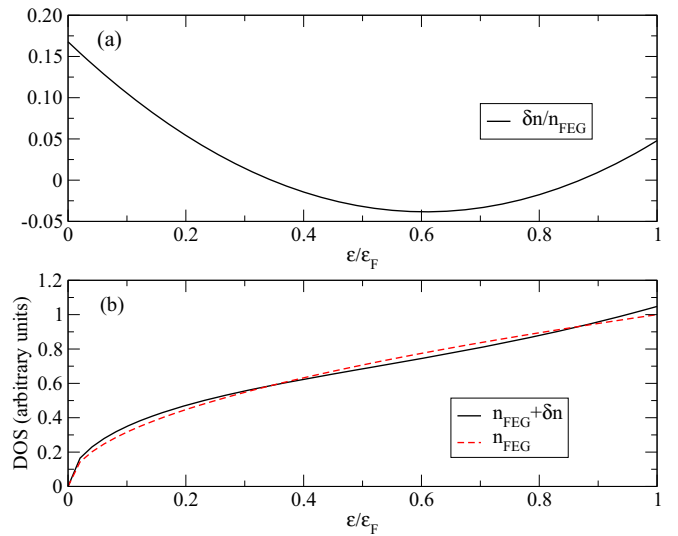
FIG. 6. (a) Function $\delta n/n_{\text{FEG}}$, where δn is the deviation from the n_{FEG} DOS induced by sp to d transfer. (b) The perturbed ($n_{\text{FEG}} + \delta n$) DOS (black continuous curve) is compared to the n_{FEG} one (red dashed curve).

where n_{FEG} is the FEG DOS given by Eq. (30) and δn the perturbation to the DOS induced by $\delta\rho(r)$. The latter reads

$$\delta n(\epsilon) = -\frac{3}{2}\frac{Z_2^0(1-\alpha)}{\epsilon_F^{3/2}}\epsilon^{1/2} - \frac{5}{2}\frac{Z_2^0\alpha}{\epsilon_F^{5/2}}\epsilon^{3/2} + \frac{7}{2}\frac{Z_2^0}{\epsilon_F^{7/2}}\epsilon^{5/2}.$$
$$(68)$$

Using $\alpha = 1.7$,

$$\frac{\delta n(\epsilon)}{n_{\text{FEG}}(\epsilon)} = \frac{Z_2^0}{3Z^*}(7(\epsilon/\epsilon_F)^2 - 8.5(\epsilon/\epsilon_F) + 2.1). \quad (69)$$

In the next section, we will see that $Z_2^0 \leqslant 0.719$, so that

$$\frac{\delta n(\epsilon)}{n_{\text{FEG}}(\epsilon)} \leqslant \frac{0.719}{9}(7(\epsilon/\epsilon_F)^2 - 8.5(\epsilon/\epsilon_F) + 2.1). \quad (70)$$

The function of ϵ/ϵ_F that appears on the right side of the preceding equation is traced on Fig. 6(a). Figure 6(b) compares the ideal n_{FEG} to the perturbed ($n_{\text{FEG}} + \delta n$) one. Except at values $\epsilon/\epsilon_F \leqslant 0.2$, $\delta n/n_{\text{FEG}}$ does not exceed 0.05.

The last step of the present work is to check the consistency of the average-atom thermal electronic energies with the value $\alpha = 1.7$.

IV. VALIDATION OF OUR AVERAGE-ATOM RESULTS

A. Case of moderate temperatures ($T \ll T_F$)

We will first discuss the case of temperatures well below Fermi temperature, at which we observed strong deviation from FEG theory with the average-atom code PARADISIO. The latter results correspond to the squares and circles in Fig. 7, respectively representing the cases of $T = 10\,000$ K and $T = 5500$ K. We compare them to the values obtained when we use Eq. (48) with $\alpha = 1.7$. Equation (48) also requires Z_2^0 values. We propose to use the fit [provided in Eq. (49)] of the values we calculated at $T = 0$ K.
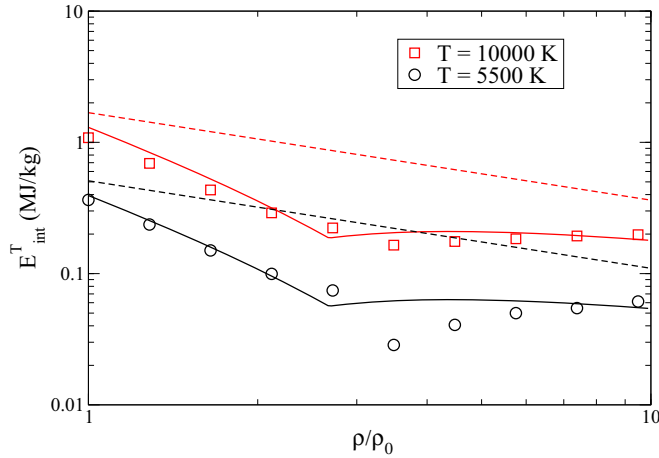
FIG. 7. Thermal electronic internal energies obtained at moderate temperatures for compressed aluminum with our average-atom code PARADISIO are compared to the curves (full lines) calculated using Eq. (48) with $\alpha = 1.7$. Squares: $T = 10^4$ K. Circles: $T = 5500$ K. Dashed lines correspond to Sommerfeld's expansion for FEG.

However, considering the choice we made concerning the electronic wave functions (i.e., asymptotic form of Bessel functions), the highest possible number of d electrons is limited. According to the degeneracy $2(2\ell + 1)$ of the band, the highest possible electron density reads

$$\rho_\ell(r, k) = \frac{1}{4\pi} 2(2\ell + 1) \frac{2k^2}{\pi} \frac{(kr)^{2\ell}}{[(2\ell + 1)!!]^2}. \quad (71)$$

Integrating over the volume yields the density of states

$$\int_V \rho_\ell(r, k)d^3r = \frac{2(2\ell + 1)}{[(2\ell + 1)!!]^2} \frac{2}{\pi} \frac{R^{2\ell+3}}{(2\ell + 3)} k^{2\ell+2}; \quad (72)$$

i.e., for $\ell = 2$, the density of states reads

$$\int_V \rho_2(r, k)d^3r = \frac{4}{315\pi} R^7 k^6, \quad (73)$$

which finally, after integration over k, gives for the maximal number of d electrons between $\epsilon = 0$ and $\epsilon_F = k_F^2/2$

$$Z_2^{\max} = \frac{4}{2205\pi}(k_F R)^7 = \frac{4}{2205\pi}\left(\frac{9\pi Z^*}{4}\right)^{7/3} = 0.719. \quad (74)$$

This value is reached at compression $\rho/\rho_0 = 2.68$, and it seems to us that this constraint will seriously limit the applicability of Eq. (48) at higher compression rates.

Figure 7 displays a comparison between the thermal internal electronic energies we obtained with PARADISIO to the values evaluated with Eq. (48), using Eq. (49) for Z_2^0 at compression $\rho/\rho_0 \leqslant 2.68$ and $Z_2^{\max} = 0.719$ above. At the lowest compression rates, applying Eq. (48) with the value $\alpha = 1.7$, PARADISIO energies are quite perfectly reproduced. The figure shows also (dashed lines) the energies obtained within the FEG approximation.

Above compression $\rho/\rho_0 \approx 3$, we observe an unexpected result. The straight lines obtained with Eq. (48) stop their
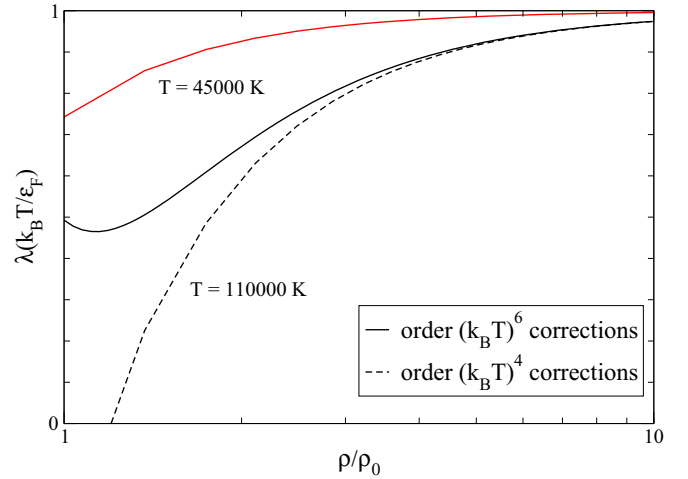
FIG. 8. Correction factor to the Coulomb contribution to energy up to order $(k_B T)^6$. Cases of $T = 45\,000$ K and $T = 110\,000$ K.

$(\rho/\rho_0)^{-\gamma_e}$ decrease because of our constraint $Z_2^0 \leqslant 0.719$. The surprising fact is that PARADISIO's energies do the same, but for slightly higher compression, so that we still observe good agreement between the code's values and those given by Eq. (48) in a density range where the latter equation starts to be more and more questionable.

B. Case of high temperatures (up to T_F)

For the purpose of comparisons up to temperatures close to the Fermi one, we expanded Eq. (48) up to order $(k_B T)^6$. At sixth order in the expansion, the thermal Coulomb part of the energy must be corrected by a function λ of the ratio $k_B T/\epsilon_F$ (see Appendix B for details about the calculation):

$$U_c^T = -\frac{\pi^2}{3}\left(\frac{k_B T}{\epsilon_F}\right)^2 \frac{Z^* Z_2^0}{R}\left(\frac{35}{9} - \frac{10}{7}\alpha\right) \times \lambda\left(\frac{k_B T}{\epsilon_F}\right), \quad (75)$$

where $\lambda(x)$ is given by

$$\begin{aligned}\lambda(x) = 1 &+ x^2 \times 3\pi^2 \frac{(-49/108 + 53\alpha/252)}{(35/9 - 10\alpha/7)} \\ &+ x^4 \times 3\pi^4 \frac{(-3047/93312 + 6205\alpha/254016)}{(35/9 - 10\alpha/7)}.\end{aligned} \quad (76)$$

Taking $\alpha = 1.7$ we get

$$\lambda(x) = 1 - 1.94978\,x^2 + 1.77569\,x^4. \quad (77)$$

We present this correction function along aluminum's rate of compression for $T = 45\,000$ K and $T = 110\,000$ K at orders $(k_B T)^4$ (dashed lines) and $(k_B T)^6$ (straight lines) in Fig. 8. At $T = 45\,000$ K, sixth-order corrections are negligible. For $T = 110\,000$ K, they become important at the lowest compression rates $\rho/\rho_0 \lesssim 3$. At densities close to ρ_0, they prevent negative corrections and consequently nonphysical positive U_c^T values. But, due to the alternate signs of the successive orders, corrections above fourth order affect the shape of the curves, as illustrated by the black straight line at $T = 110\,000$ K. In this latter case, sixth-order corrections create a minimum in the vicinity of ρ_0. Higher order corrections will
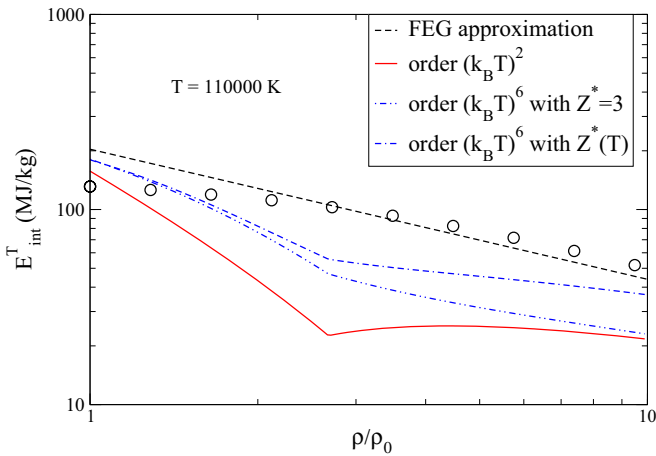
FIG. 9. Thermal electronic energy at $T = 110\,000$ K. Circles: values from PARADISIO code. Dashed line: order $(k_B T)^2$ of Sommerfeld's expansion for FEG. Straight line: Eq. (48). Double-dot-dash line: Eq. (75) with $Z^* = 3$. Dot-double-dash line: Eq. (75) using the Thomas-Fermi ionization expression for Z^*.

introduce oscillations. However, in the case of aluminum, the observed minimum occurs in a density range where electron-electron contributions to the thermal energy are rather low in comparison with band structure contributions.

Figure 9 details fourth- and sixth-order corrections to thermal energies at temperature $T = 110\,000$ K. The circles are the average-atom calculations. We notice that, at this temperature, the FEG behavior is recovered. Coulomb contributions vanish rapidly as temperature rises. Clearly we encountered some difficulty to reproduce this effect. At the lowest densities (i.e., at compression less than 4) one can suspect the necessity of considering higher order terms in the temperature expansions. But at compression approaching 10, the sixth-order corrections are rather small even at this temperature, and so will be higher order terms. However, in such conditions, ionization by the means of compression
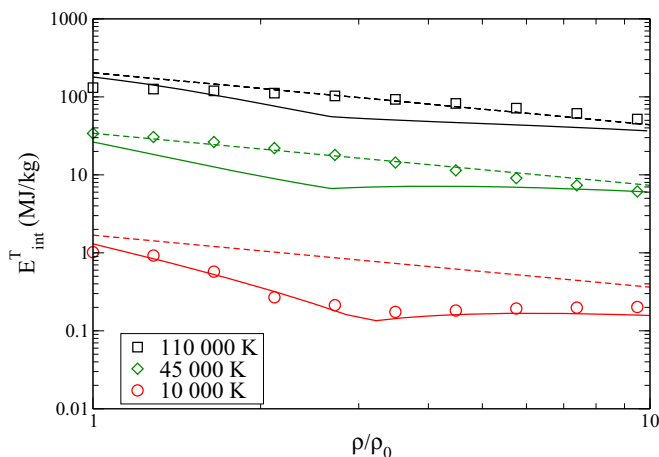
FIG. 10. Thermal electronic internal energies obtained at high temperatures. The symbols represent PARADISIO values. Squares: $T = 110\,000$ K. Diamonds: $T = 45\,000$ K. Straight lines: with Eq. (75). Dashed lines: Sommerfeld's expansion for FEG, limited at order $(k_B T)^2$. The case of $T = 10\,000$ K is also recalled (circles).

and probably also by temperature is highly possible. In order to quantify the consequence of such effects, we replaced $Z^* = 3$ by the Thomas-Fermi ionization number [46] and obtained the double-dash-dot curve, which "improves" slightly the double-dot-dash one at the highest compression. Nevertheless, it seems difficult to obtain more than qualitative agreement with average-atom PARADISIO results at high temperature. Figure 10 presents the best results we can obtain for the time being. But we must remind that the case of high temperatures is beyond the initial scope of our work.

V. SUMMARY

Aluminum belongs to the class of simple metals, characterized by valence bands forming nearly free electron gases. This view is supported by valence density of states calculations, which confirm the $n(\epsilon) \propto \epsilon^{1/2}$ FEG-like behavior. The discrepancy observed between some experimental values, such as the electronic Grüneisen constant and the one deduced from FEG assumption, is, in the case of aluminum, explained by strong electron-phonon coupling. Our recent average-atom calculations of thermal contributions to electronic internal energies along with temperature and compression suggest that there is also an electronic reason for the high experimental electronic value of the Grüneisen parameter.

Internal energy contains a band structure term but also a contribution from electron-electron Coulomb interactions. Within the FEG approach for the valence band, the latter does not contribute to thermal energy. However, our PARADISIO calculations showed that a small part of the valence electrons transfer to a $3d$ band that moved below Fermi energy by the means of the compression. We expected the presence of d-like electrons among the $Z^* = 3$ valence ones to bring contributions from Coulomb interactions. The aim of the present work was to examine this possibility.

We therefore developed a simple analytic model for aluminum's valence band in terms of a FEG perturbed by sp to d transfer, and obtained, using Sommerfeld's expansion method, an analytic expression for Coulomb contribution to thermal energies, as a function of the fraction α of d electrons coming from the $2p$ band. The value $\alpha = 1.7$ was obtained from $T = 0$ K energies deduced from Hugoniot data. Using this value, our simple model perfectly accounts for the average-atom thermal energies at moderate temperatures ($T \leqslant 10\,000$ K) and therefore validates them, which was our main objective. Besides that, our work also points out the role of sp to d transfer in aluminum's thermal electronic properties under compression. Particularly, this electronic transfer induces high electronic Grüneisen constant, well above the $\gamma_e^{\text{FEG}} = 2/3$ FEG's value. However, at $\rho = \rho_0$, we found a large range of possible values for α. At $\rho = \rho_0$, we therefore conclude that sp to d transfer may contribute to the high value of the electronic Grüneisen constant together with strong electron-phonon coupling, whose role is unquestionable according to experiment.

Despite the fact that high temperatures are out of the scope of our paper, we tested the validity of our simplified approach at temperatures $T \gg 10\,000$ K and proposed some possible improvements such as inclusion of higher order terms in the

temperature expansion, or accounting for thermal ionization, with moderate success.

Besides the fact that we have explained cold energy, the electronic Grüneisen parameter, and average-atom thermal energies by electron transfer from sp bands to a d one that overlaps the former near ϵ_F, our work may be useful for performing fast evaluation of electronic thermal contributions to EOS of other metals with FEG-type valence bands beyond the usual Sommerfeld expansion.

APPENDIX A: THE AVERAGE-ATOM CODE PARADISIO

PARADISIO [4] code is based on Liberman's relativistic quantum-average-atom model INFERNO [30] (see also Ref. [3]). INFERNO considers an atom as a point nucleus surrounded by its Z electrons and places it at the center of a spherical cavity buried in a jellium, i.e., a uniform distribution of positive charges which takes place of the surrounding ions, and a constant electron distribution that ensures electrical neutrality. Electrical neutrality inside the cavity is imposed too. Electronic structure is then computed on a self-consistent way. The only needed parameters are the atomic number Z, density ρ, and temperature T.

As in the main text, atomic units where $e = \hbar = m = 1$ are used throughout the Appendix. We also choose to use speed c of light instead of hyperfine structure constant $\alpha = \frac{e^2}{8\pi\epsilon_0 a_0}$.

In a spherically symmetric potential, the one-electron wave functions, solutions of the Dirac equation, are of the form

$$\psi_s(\vec{r}) \equiv \psi_{j\ell m}(\vec{r}) = \begin{pmatrix} \frac{1}{r}F(r)\Omega_{j\ell m}(\theta, \phi) \\ -\frac{i}{r}G(r)\Omega_{j\ell' m}(\theta, \phi) \end{pmatrix}, \quad (A1)$$

where $\Omega_{j\ell m}$ and $\Omega_{j'\ell m}$ are two spinors. j, ℓ, and m are quantum numbers associated respectively with the total angular momentum J, to the orbital angular momentum L, and its projection L_z. We define the quantum number ℓ' by

$$\ell' = \begin{cases} \ell + 1 & \text{if } j = \ell + 1/2, \\ \ell - 1 & \text{if } j = \ell - 1/2. \end{cases} \quad (A2)$$

The radial functions F and G verify the equations

$$\frac{dF}{dr} = -\frac{\kappa}{r}F(r) - \frac{V_{\text{eff}}(r) - c^2 - \epsilon}{c}G(r),$$

$$\frac{dG}{dr} = \frac{V_{\text{eff}}(r) + c^2 - \epsilon}{c}F(r) + \frac{\kappa}{r}G(r), \quad (A3)$$

where

$$\begin{array}{ll} \kappa = -(\ell + 1) & \text{for } j = \ell + 1/2, \\ \kappa = \ell & \text{for } j = \ell - 1/2. \end{array} \quad (A4)$$

The potential is assumed to be constant outside the cavity $[V(r) = V_\infty$ for $r \geqslant R]$. Therefore, the solutions of Dirac equation are known for $r \geqslant R$, and the equation has to be solved for $r \leqslant R$. The inside and outside solutions are matched at $r = R$.

The number of bound electrons reads

$$N_{\text{bound}} = \sum_b X_b f(\epsilon_b) \quad (A5)$$

and the number of free electrons

$$N_{\text{free}} = \sum_\kappa \int_0^\infty X_\kappa(\epsilon)f(\epsilon)d\epsilon, \quad (A6)$$

where $f(\epsilon_i)$ is the Fermi-Dirac occupation of state i of either the bound discrete energy ϵ_b or the continuum free one denoted by ϵ.

The factor X_i $(i = b, \kappa)$ is

$$X_i = \int_{r \leqslant R} \psi_i^*(\vec{r})\psi_i(\vec{r})d^3r \quad (A7)$$

and one has

$$X_\kappa(\epsilon) = 2|\kappa| \int_0^R [F^2(r) + G^2(r)]dr, \quad (A8)$$

where

$$\epsilon = c^2\sqrt{1 + \frac{k^2}{c^2}} \quad \text{or} \quad k = \sqrt{2\epsilon\left(1 + \frac{\epsilon}{2c^2}\right)}. \quad (A9)$$

The chemical potential is obtained from the electroneutrality condition

$$N_{\text{bound}} + N_{\text{free}} = Z, \quad (A10)$$

Z being the atomic number of the considered element. In the usual regime [typically $\mu/(k_B T) = \beta\mu$ less than 250], the Fermi distribution is far from the step function. In that case, Eq. (A6) can be split in two parts:

$$N_{\text{free},0} = \sum_\kappa \int_0^{\epsilon_m} X_\kappa(\epsilon)f(\epsilon)d\epsilon \quad (A11)$$

and

$$N_{\text{free},1} = \sum_\kappa \int_{\epsilon_m}^\infty X_\kappa(\epsilon)e^{-\beta(\epsilon-\mu)}d\epsilon \quad (A12)$$

with $\epsilon_m = \max(0, \mu + 10/\beta)$. In Eq. (A12), we can assume that $X_\kappa(\epsilon)$ can be approximated using the ideal wave functions of an electron gas,

$$F(r) = k\sqrt{\frac{k}{\pi\epsilon}}j_\ell(kr),$$

$$G(r) = k\sqrt{\frac{k}{\pi\epsilon}}j_{\ell'}(kr), \quad (A13)$$

and we get finally in that case

$$X_\kappa(\epsilon) = \frac{1 + \epsilon/c^2}{\pi^2 k}k^2\left(\frac{4}{3}\pi R^3\right), \quad (A14)$$

with the maximal orbital quantum number $\ell_m \approx k_m R$, k_m being related to ϵ_m through the second identity of Eq. (A9).

The model imposes $F = G = 0$ at $r = 0$ and $r \to \infty$. Outside the cavity, the radial functions F and G satisfying those boundary conditions are, for bound states, modified Bessel functions of the third kind [47], exponentially decreasing, and, for free states, combinations of Bessel functions of the first and second kinds, with decreasing amplitudes as $r \to \infty$.

Outside the cavity we have, for $\epsilon < V_\infty$ (bound states)

$$F(r) = a_0 c \frac{k}{V_\infty - \epsilon}r K_{\ell+1/2}(kr),$$

$$G(r) = a_0 r K_{\ell'+1/2}(kr), \quad (A15)$$

where $K_{n+1/2}$ (n being an integer) are modified Bessel functions of the third kind and a_0 is the normalization constant such that:

$$\int_0^\infty [F^2(r) + G^2(r)]dr = 1. \quad (A16)$$

Outside the cavity we have, for $\epsilon > V_\infty$ (free states)

$$F(r) = b_0 c \frac{k}{\epsilon - V_\infty} r[\cos(\delta_\ell) j_\ell(kr) - \sin(\delta_\ell) n_\ell(kr)],$$

$$G(r) = b_0 r[\cos(\delta_\ell) j_{\ell'}(kr) - \sin(\delta_\ell) n_{\ell'}(kr)], \quad (A17)$$

where the normalization factor b_0 and the wave number k are

$$b_0 = \sqrt{\frac{2}{\pi}} \frac{k}{\sqrt{1 + \frac{c^2 k^2}{(\epsilon - V_\infty)^2}}}$$

$$k = \sqrt{2(V_\infty - \epsilon)\left(1 - \frac{(V_\infty - \epsilon)}{2c^2}\right)}.$$

The matching of the solutions at the cavity radius provides the spectrum of bound energies and the phase shifts δ_ℓ.

The electronic structure (bound and free states) being known, the thermodynamic quantities can be calculated. We compute the internal energy as

$$E = K + U_{c,1} + U_{c,2} + E_{\text{xc}}^{\text{int}}, \quad (A18)$$

where the kinetic energy K reads

$$K = \sum_b f(\epsilon_b)(\epsilon_b - V_\infty)X_b$$

$$+ \sum_\kappa \int_0^\infty f(\epsilon)(\epsilon - V_\infty)X_\kappa(\epsilon)d\epsilon$$

$$- \int_{r \leqslant R} \rho(r)[V_{\text{eff}}(r) - V_\infty]d^3r \quad (A19)$$

with

$$\rho(r) = \frac{1}{4\pi r^2} \sum_{i=b,k} f(\epsilon_i)\big[F_i^2(r) + G_i^2(r)\big]. \quad (A20)$$

The quantity V_{eff} represents the effective potential

$$\begin{aligned} V_{\text{eff}}(r) &= V_c(r) + V_{\text{xc}}(r) - \nu \quad \text{if } r \leqslant R, \\ V_{\text{eff}}(r) &= V_\infty \quad \text{if } r > R \end{aligned} \quad (A21)$$

with

$$V_c(r) = -\frac{Z}{r} + \int_{r' \leqslant R} \frac{\rho(r')}{|\vec{r} - \vec{r}'|} d^3r', \quad (A22)$$

$$V_{\text{xc}}(r) = \mu_{\text{xc}}[\rho(r), T], \quad (A23)$$

and

$$V_\infty(r) = \mu_{\text{xc}}[\bar{\rho}, T], \quad (A24)$$

where $\bar{\rho}$ is the density of the jellium. The exchange-correlation chemical potential functional is

$$\mu_{\text{xc}}[n, T] = \frac{\partial}{\partial n} n f_{\text{xc}}[n, T]\Big|_n, \quad (A25)$$

where f_{xc} is the exchange-correlation free-energy density functional. PARADISIO uses the finite-temperature exchange-correlation functionals of Karasiev *et al.* [48].

Finally, the parameter ν in Eq. (A21) is

$$\nu = f_{\text{xc}}[\rho(R), T] - \mu_{\text{xc}}[\bar{\rho}, T] + \frac{\bar{\rho}}{\rho(R)}(\mu_{\text{xc}}[\bar{\rho}, T]$$

$$- f_{\text{xc}}[\bar{\rho}, T]). \quad (A26)$$

The quantity $U_{c,1}$ represents the electron-nucleus Coulomb interaction energy

$$U_{c,1} = -\int_{r \leqslant R} \frac{\rho(r)}{r} d^3r \quad (A27)$$

and $U_{c,2}$ the electron-electron Coulomb interaction energy

$$U_{c,2} = \frac{1}{2} \iint_{r \leqslant R} \frac{\rho(r)\rho(r')}{|\vec{r} - \vec{r}'|} d^3r\, d^3r'. \quad (A28)$$

$E_{\text{xc}}^{\text{int}}$ represents the exchange-correlation electron-electron energy

$$E_{\text{xc}}^{\text{int}} = \int_{r \leqslant R} \rho(r)\epsilon_{\text{xc}}[\rho(r), T]d^3r, \quad (A29)$$

with

$$\epsilon_{\text{xc}}[n, T] = \frac{\partial}{\partial \beta} \beta f_{\text{xc}}[n, T]\Big|_n. \quad (A30)$$

More details can be found in Ref. [31]. In particular, a relativistic stress-tensor formula is given for the pressure due to bound and free electrons.

APPENDIX B: FOURTH- AND SIXTH-ORDER TEMPERATURE EXPANSION OF COULOMB CONTRIBUTION TO ENERGY

1. Up to sixth-order term in the temperature expansion of the chemical potential

We are seeking for a relation

$$\mu - \epsilon_F = a(k_B T)^2 + b(k_B T)^4 + c(k_B T)^6. \quad (B1)$$

In the absence of thermal ionization, the total number of electrons remains unchanged at finite temperature T so that

$$\int_0^{\epsilon_F} n(\epsilon)d\epsilon = \int_0^\infty n(\epsilon)f(\epsilon)d\epsilon. \quad (B2)$$

Consequently, using Eq. (7) with $H(\epsilon) = n(\epsilon)$,

$$\int_{\epsilon_F}^\mu n(\epsilon)d\epsilon + \frac{\pi^2}{6}(k_B T)^2 n^{(1)}(\mu) + \frac{7\pi^4}{360}(k_B T)^4 n^{(3)}(\mu)$$

$$+ \frac{31\pi^6}{15120}(k_B T)^6 n^{(5)}(\mu) \cdots = 0, \quad (B3)$$

where

$$n^{(i)}(\mu) = \frac{d^i n(\epsilon)}{d\epsilon^i}\Big|_\mu.$$

$n(\epsilon)$ is then expanded as a power series of $(\epsilon - \epsilon_F)$,

$$n(\epsilon) = n(\epsilon_F) + (\epsilon - \epsilon_F)n^{(1)}(\epsilon_F) + \frac{1}{2}(\epsilon - \epsilon_F)^2 n^{(2)}(\epsilon_F)$$

$$+ \frac{1}{6}(\epsilon - \epsilon_F)^3 n^{(3)}(\epsilon_F) + \cdots, \quad (B4)$$

and used to obtain the integral between ϵ_F and μ, as well as the values at μ of the density-of-state's derivatives. Regrouping contributions proportional to $(k_BT)^2$, $(k_BT)^4$, and $(k_BT)^6$, and introducing the notation $n_F^{(i)} = n^{(i)}(\epsilon_F)$,

$$(k_BT)^2\left(an_F + \frac{\pi^2}{6}n_F^{(1)}\right) + (k_BT)^4\left(bn_F + \frac{a^2}{2}n_F^{(1)} + \frac{\pi^2}{6}an_F^{(2)} + \frac{7\pi^4}{360}n_F^{(3)}\right)$$

$$+ (k_BT)^6\left(cn_F + abn_F^{(1)} + \frac{a^3 + b\pi^2}{6}n_F^{(2)} + \frac{\pi^2a^2}{12}n_F^{(3)} + \frac{7\pi^4}{360}an_F^{(4)} + \frac{31\pi^6}{15120}n_F^{(5)}\right) + O(k_BT)^8 = 0 \qquad (B5)$$

gives a relation that applies to any temperature, so that coefficients of $(k_BT)^2$, $(k_BT)^4$, and $(k_BT)^6$ must be equal to zero. Since the DOS for the FEG $n(\epsilon)$ varies as $\epsilon^{1/2}$, one finally gets $a = -\frac{\pi^2}{12\,\epsilon_F}$, $b = -\frac{\pi^4}{80\,\epsilon_F^3}$, and $c = -\frac{247\pi^6}{25920\,\epsilon_F^5}$.

2. Higher orders in the temperature expansion of electronic densities

We go back to the temperature expansion for partial electronic density,

$$\rho_\ell(r) = \rho_\ell^0(r) + \int_{\epsilon_F}^{\mu} \rho_\ell(r, \epsilon)d\epsilon + \frac{\pi^2}{6}(k_BT)^2\left.\frac{\partial\rho_\ell(r, \epsilon)}{\partial\epsilon}\right|_{\mu}$$

$$+ \frac{7\pi^4}{360}(k_BT)^4\left.\frac{\partial^3\rho_\ell(r, \epsilon)}{\partial\epsilon^3}\right|_{\mu} + \frac{31\pi^6}{15120}(k_BT)^6\left.\frac{\partial^5\rho_\ell(r, \epsilon)}{\partial\epsilon^5}\right|_{\mu} + O(k_BT)^8. \qquad (B6)$$

The integral and the derivatives in the preceding equation are obtained using the following expansion of $\rho_\ell(r, \epsilon)$ as a power series of $(\epsilon - \epsilon_F)$:

$$\rho_\ell(r, \epsilon) = \rho_\ell(r, \epsilon_F) + \sum_{n=1}^{5}\frac{1}{n!}(\epsilon - \epsilon_F)^n\left.\frac{d^n\rho_\ell(r, \epsilon)}{d\epsilon^n}\right|_{\mu} + O(\epsilon - \epsilon_F)^6. \qquad (B7)$$

Replacing $(\mu - \epsilon_F)$ by its expansion

$$\mu - \epsilon_F = a(k_BT)^2 + b(k_BT)^2 + c(k_BT)^6, \qquad (B8)$$

we obtain

$$\int_{\epsilon_F}^{\mu} \rho_\ell(r, \epsilon)d\epsilon = (k_BT)^2 a\rho_\ell(r, \epsilon_F) + (k_BT)^4\left\{b\rho_\ell(r, \epsilon_F) + \frac{a^2}{2}\left.\frac{\partial\rho_\ell(r, \epsilon)}{\partial\epsilon}\right|_{\epsilon_F}\right\}$$

$$+ (k_BT)^6\left\{c\rho_\ell(r, \epsilon_F) + ab\left.\frac{\partial\rho_\ell(r, \epsilon)}{\partial\epsilon}\right|_{\epsilon_F}\right\} + O(k_BT)^8, \qquad (B9)$$

$$\frac{\pi^2}{6}(k_BT)^2\left.\frac{\partial\rho_\ell(r, \epsilon)}{\partial\epsilon}\right|_{\mu} = \frac{\pi^2}{6}(k_BT)^2\left.\frac{\partial\rho_\ell(r, \epsilon)}{\partial\epsilon}\right|_{\epsilon_F} + \frac{\pi^2}{6}(k_BT)^4 a\left.\frac{\partial^2\rho_\ell(r, \epsilon)}{\partial\epsilon^2}\right|_{\epsilon_F}$$

$$+ (k_BT)^6\left\{\frac{\pi^2}{6}b\left.\frac{\partial^2\rho_\ell(r, \epsilon)}{\partial\epsilon^2}\right|_{\epsilon_F} + \frac{\pi^2}{12}a^2\left.\frac{\partial^3\rho_\ell(r, \epsilon)}{\partial\epsilon^3}\right|_{\epsilon_F}\right\} + O(k_BT)^8, \qquad (B10)$$

$$\frac{7\pi^4}{360}(k_BT)^4\left.\frac{\partial^3\rho_\ell(r, \epsilon)}{\partial\epsilon^3}\right|_{\mu} = \frac{7\pi^4}{360}(k_BT)^4\left.\frac{\partial^3\rho_\ell(r, \epsilon)}{\partial\epsilon^3}\right|_{\epsilon_F} + \frac{7\pi^4}{360}(k_BT)^6 a\left.\frac{\partial^4\rho_\ell(r, \epsilon)}{\partial\epsilon^4}\right|_{\epsilon_F} + O(k_BT)^8, \qquad (B11)$$

and

$$\frac{31\pi^6}{15120}(k_BT)^6\left.\frac{\partial^5\rho_\ell(r, \epsilon)}{\partial\epsilon^5}\right|_{\mu} = \frac{31\pi^6}{15120}(k_BT)^6\left.\frac{\partial^5\rho_\ell(r, \epsilon)}{\partial\epsilon^5}\right|_{\epsilon_F} + O(k_BT)^8. \qquad (B12)$$

Replacing a, b, and c by their values $a = -\frac{\pi^2}{12\epsilon_F}$, $b = -\frac{\pi^4}{80\epsilon_F^3}$, and $c = -\frac{247\pi^6}{25920\,\epsilon_F^5}$ and using the relation

$$\left.\frac{\partial^n\rho_\ell(r, \epsilon)}{\partial\epsilon^n}\right|_{\epsilon_F} = \rho_\ell(r, \epsilon_F)\frac{\prod_{i=1}^{n}(2\ell + 3 - 2i)}{(2\epsilon_F)^n}, \qquad (B13)$$

the thermal contribution $\rho_\ell^T(r)$ to the partial electron density finally reads

$$\rho_\ell^T(r) = \epsilon_F\rho_\ell(r, \epsilon_F) \times \ell\left\{\frac{X^2}{6} + \frac{14\,\ell^2 - 31\,\ell - 1}{720}X^4 + \frac{(372\,\ell^4 - 3084\,\ell^3 + 7791\,\ell^2 - 5767\,\ell - 1782)}{181440}X^6\right\} + O(X^8), \quad (B14)$$

where we have introduced

$$X = \frac{\pi k_B T}{\epsilon_F}. \tag{B15}$$

We get then, respectively for $\ell = 0$, 1, and 2,

$$\rho_0^T(r) = 0, \tag{B16}$$

$$\rho_1^T(r) = \epsilon_F \, \rho_1(r, \epsilon_F) \left\{ \frac{X^2}{6} - \frac{X^4}{40} - \frac{247}{18144} X^6 + O(X^8) \right\}, \tag{B17}$$

and

$$\rho_2^T(r) = \epsilon_F \, \rho_2(r, \epsilon_F) \left\{ \frac{X^2}{3} - \frac{7}{360} X^4 - \frac{109}{11340} X^6 + O(X^8) \right\}. \tag{B18}$$

3. Thermal electron-electron Coulomb contribution to energy up to order $(k_B T)^6$

To obtain these contributions we need the integrals

$$(4\pi)^2 \int_0^R \rho_1(r, \epsilon_F) \int_r^R \rho_{\text{FEG}} r' dr' \, r^2 dr + (4\pi)^2 \int_0^R \rho_{\text{FEG}} \int_r^R \rho_1(r', \epsilon_F) r' dr' \, r^2 dr = -\alpha Z_2(T) Z^* \frac{20}{7R \, \epsilon_F}, \tag{B19}$$

and

$$(4\pi)^2 \int_0^R \rho_2(r, \epsilon_F) \int_r^R \rho_{\text{FEG}} r' dr' \, r^2 dr + (4\pi)^2 \int_0^R \rho_{\text{FEG}} \int_r^R \rho_2(r', \epsilon_F) r' dr' \, r^2 dr = Z_2(T) Z^* \frac{35}{9R \, \epsilon_F}, \tag{B20}$$

where we have introduced a temperature-dependent occupation number $Z_2(T)$ for the d band. Indeed, as long as no thermal ionization occurs, the total number Z^* of electrons in the valence band is constant. However, distributions of these electrons on the s, p, and d bands change with increasing temperatures. The number of d electrons reads

$$Z_2(T) = \int_0^{\epsilon_F} n_2(\epsilon) d\epsilon + \int_{\epsilon_F}^{\mu} n_2(\epsilon) d\epsilon, \tag{B21}$$

with

$$n_2(\epsilon) = \frac{7 Z_2^0}{2 \epsilon_F^{7/2}} \epsilon^{5/2}. \tag{B22}$$

We need to expand $Z_2(T)$ up to order $(k_B T)^4$

$$Z_2(T) = Z_2^0 \left(1 - \frac{7}{24} X^2 - \frac{77}{5760} X^4 + O(X^6) \right). \tag{B23}$$

The temperature expansion of the thermal contribution of electron-electron Coulomb contributions to the internal energy follows straightforwardly:

$$U_c^T = -\frac{Z_2^0 Z^*}{R} \left\{ \frac{1}{3} \left(\frac{\pi k_B T}{\epsilon_F} \right)^2 \left(\frac{35}{9} - \alpha \frac{10}{7} \right) + \left(\frac{\pi k_B T}{\epsilon_F} \right)^4 \left(-\frac{49}{108} + \alpha \frac{53}{252} \right) + \left(\frac{\pi k_B T}{\epsilon_F} \right)^6 \left(-\frac{3047}{93312} + \alpha \frac{6205}{254016} \right) \right\} + O(k_B T)^8. \tag{B24}$$

We can notice that the introduction of a temperature dependent d band occupation number does not affect the $(k_B T)^2$ expansion presented in the main text.

[1] M. D. Knudson, M. P. Desjarlais, and A. Pribram-Jones, Adiabatic release measurements in aluminum between 400 and 1200 GPa: Characterization of aluminum as a shock standard in the multimegabar regime, Phys. Rev. B **91**, 224105 (2015).

[2] M. A. Kadatskiy, and K. V. Khishchenko, Comparison of Hugoniots calculated for aluminum in the framework of three quantum-statistical models, J. Phys. Conf. Ser. **643**, 012079 (2015).

[3] B. Wilson, A. Sonnad, P. Sterne, and W. Isaacs, Purgatorio - a new implementation of the Inferno algorithm, J. Quant. Spectrosc. Radiat. Transfer **99**, 658 (2006).

[4] M. Pénicaud, An average atom code for warm matter: Application to aluminum and uranium, J. Phys.: Condens. Matter **21**, 095409 (2009).

[5] J.-C. Pain, Equation-of-state model for shock compression of hot dense matter, Phys. Lett. A **362**, 120 (2007).

[6] R. Piron, and T. Blenski, Variational-average-atom-in-quantum-plasmas (VAAQP) code and virial theorem. Equation of state and shock-Hugoniot calculation for warm dense Al, Fe, Cu, and Pb, Phys. Rev. E **83**, 026403 (2011).

[7] G. Faussurier, C. Blancard, P. Cossé, and P. Renaudin, Equation of state, transport coefficients, and stopping power of dense

plasmas from average-atom model self-consistent approach for astrophysical and laboratory plasmas, Phys. Plasmas **17**, 052707 (2010).

[8] S. Mazevet, and G. Zérah, *Ab Initio* Simulations of the *K*-edge shift along the Aluminum Hugoniot, Phys. Rev. Lett. **101**, 155001 (2008).

[9] J. Clerouin, P. Noiret, V. N. Korobenko, and A. D. Rakhel, Direct measurements and *ab initio* expanded fluid aluminum in the metal-nonmetal transition range, Phys. Rev. B **78**, 224203 (2008).

[10] M. P. Surh, T. W. Barbee III, and L. H. Yang, First principles Molecular Dynamics of Dense Plasmas, Phys. Rev. Lett. **86**, 5958 (2001).

[11] D. V. Minakov, P. R. Levaskov, K. V. Khishchenko, and V. E. Fortov, Quantum molecular dynamics simulation of shock wave experiments in aluminum, J. Appl. Phys. **115**, 223512 (2014).

[12] X. Gao, L. Chen, R. Valencia, W. Xia, W. Gao, X.-Y. Han, J.-M. Li, and P. Zhang, *Ab initio* study of thermodynamically consistent equation of state of warm dense aluminum plasma, Phys. Plasmas **23**, 092710 (2016).

[13] T. S. Sjostrom, S. Crockett, and S. Rudin, Multiphase aluminum equation of state via density functional theory, Phys. Rev. B **94**, 144101 (2016).

[14] F. Lambert, J. Clérouin, and G. Zérah, Very-high-temperature molecular dynamics, Phys. Rev. E **73**, 016403 (2006).

[15] S. Zhang, H. Wang, W. Kang, P. Zhang, and X. He, Extended application of Kohn-Sham first-principles molecular dynamics method with plane wave approximation at high energy - From cold materials to hot dense plasmas, Phys. Plasmas **23**, 042707 (2016).

[16] D. A. Young, J. K. Wolford, F. J. Rogers, and K. S. Holian, Theory of the aluminum shock equation of state to 104 Mbar, Phys. Lett. A **108**, 157 (1985).

[17] F. J. Rogers and D. A. Young, Validation of the activity expansion method with ultrahigh pressure shock equation of state, Phys. Rev. E **56**, 5876 (1997).

[18] I. V. Lomonosov, Multi-phase equation of state for aluminum, in *Shock Compression of Condensed Matter - 2007: Proceedings of the Conference of the American Physical Society Topical Group on Shock Compression of Condensed Matter*, June 2007, Waikoloa, HI, edited by M. Elert, M. D. Furnish, R. Chau, N. Holmes, and J. Nguyen, AIP Conf. Proc. No. 955 (AIP, New York, 2007), p. 63.

[19] R. Davidov, V. Antonov, and N. Kalinin, Equation of State for simulation of nanosecond laser ablation aluminum in water and air, J. Phys. Conf. Ser. **643**, 012107 (2015).

[20] B. F. Rozsnyai, J. R. Albritton, D. A. Young, V. N. Sonnad, and D. A. Liberman, Theory and experiment for ultrahigh pressure shock Hugoniots, Phys. Lett. A **291**, 226 (2001).

[21] P. Renaudin, C. Blancard, J. Clérouin, G. Faussurier, P. Noiret, and V. Recoules, Aluminum Equation-of State Data in the Warm Dense Matter Regime, Phys. Rev. Lett. **91**, 075002 (2003).

[22] K. P. Driver, F. Soubiran, and B. Militzer, Path integral Monte Carlo simulations of warm dense aluminum, Phys. Rev. E **97**, 063207 (2018).

[23] Z. Lin, L. V. Zhigilei, and V. Celli, Electron-phonon coupling and electron heat capacity of metals under conditions of strong electron-phonon nonequilibrium, Phys. Rev. B **77**, 075133 (2008).

[24] B. H. Billings and D. E. Gray, *American Institute of Physics Handbook*, 3rd ed. (McGraw-Hill, New York, 1972).

[25] S. Nie, X. Wang, H. Park, R. Clinite, and J. Cao, Measurement of the Electronic Grüneisen Constant Using Femtosecond Electron Diffraction, Phys. Rev. Lett. **96**, 025901 (2006).

[26] J. G. Collins, G. K. White, and C. A. Swenson, The thermal expansion of aluminum below 35 K, J. Low Temp. Phys. **10**, 69 (1973).

[27] D. C. Wallace, Theoretical calculation of the electronic thermal expansion of simple metals, J. Appl. Phys. **41**, 5055 (1970).

[28] A. Giri, J. T. Gaskins, L. Li, Y.-S. Wang, O. V. Prezhdo, and P. E. Hopkins, First-principles determination of the ultrahigh electrical and thermal conductivity in free-electron metals via pressure tuning the electron-phonon coupling factor, Phys. Rev. B **99**, 165139 (2019).

[29] H. Dagistanli, Calculated pressure induced fcc-hcp phase transition in aluminum, Bitlis Eren Univ. J. Sci. Technol. **3**, 6 (2013).

[30] D. A. Liberman, Self-consistent field model for condensed matter, Phys. Rev. B **20**, 4981 (1979).

[31] N. Wetta, J.-C. Pain, and O. Heuzé, D'Yakov-Kontorovich instability of shock waves in hot plasmas, Phys. Rev. E **98**, 033205 (2018).

[32] A. Sommerfeld, Zur Elektronentheorie der Metalle auf Grund der Fermischen Statistik, Z. Phys. **57**, 1 (1928).

[33] N. W. Ashcroft and N. D. Mermin, in *Solid State Physics*, (Thomson Learning, Stamford, CT, 1976), p. 760.

[34] M. Selmke, The Sommerfeld Expansion, https://photonicsdesign.jimdo.com/pdfs/

[35] M. H. Rice, R. G. McQueen, and J. M. Walsh, Compression of Solids by Strong Shock Waves, in *Solid State Physics*, edited by F. Seitz and D. Turnbull (Academic, New York, 1958), Vol. 6, pp. 1–63.

[36] R. Grover, R. N. Keeler, F. J. Rogers, and G. C. Kennedy, On the compressibilty of the alkali metals, J. Phys. Chem. Solids **30**, 2091 (1969).

[37] L. V. Al'tshuler, Use of shock waves in high-pressure physics, Usp. Fiz. Nauk. **85**, 197 (1965) [Sov. Phys. Usp. **8**, 52 (1965)].

[38] L. V. Al'tshuler, S. E. Brusnikin, and E. A. Kuz'menkov, Isotherms and Grüneisen functions for 25 metals, J. Appl. Mech. Tech. Phys. **28**, 129 (1987).

[39] N. E. Phillips, Heat Capacity of Aluminum between 0.1 K and 0.4 K, Phys. Rev. **114**, 676 (1959).

[40] L. Burakovsky and D. L. Preston, Analytic model of the Grüneisen parameter all densities, J. Phys. Chem. Solids **65**, 1581 (2004).

[41] M. H. G. Jacobs and R. Schmid-Fetzer, Thermodynamic properties and equations of state of fcc aluminum and bcc iron, derived from a lattice vibrational method, Phys. Chem. Miner. **37**, 721 (2010).

[42] C. Nie, B. Zong, and J. Wang, A comparative study of Burakovsky's and Jacobs's volume dependence Grüneisen parameter for fcc aluminum, Physica B **468–469**, 7 (2015).

[43] G. I. Kerley, User's Manual for Panda II: A Computer Code for Calculating Equations of State, Sandia National Laboratories Report No. SANS88-2291, 1991 (unpublished).

[44] S. L. Thompson and H. S. Lauson, Improvement in the Chart-D Radiation-Hydrodynamic Code III: Revised Analytic Equations of State, Sandia National Laboratories Report No. SC-RR-710714, 1972 (unpublished).

[45] Aluminum Hugoniot data from http://www.ihed.ras.ru/rusbank/

[46] R. M. More, Atomic Physics in Internal Confinement Fusion, Los Alamos National Laboratory Report. No UCRL-84991, 1981 (unpublished).

[47] M. Abramowitz and I. A. Stegun, *Handbook of Mathematical Functions, Applied Mathematics Series 55* (U.S. Government Printing Office, Washington, D.C., 1964).

[48] V. V. Karasiev, T. Sjostrom, J. Dufty, and S. B. Trickey, Accurate Homogeneous Electron Gas Exchange-Correlation Free Energy for Local Spin-Density Calculations, Phys. Rev. Lett. **112**, 076403 (2014).